Elastic properties of the nematic phase in hard ellipsoids of short aspect ratio

S. Heymans[1] and T. Schilling[2]
[1]*Université du Luxembourg, Theory of Soft Condensed Matter, Physics and Materials Sciences Research Unit, L-1511 Luxembourg, Luxembourg*
[2]*Institute of Physics, University of Freiburg, Hermann-Herder-Strasse 3, D-79104 Freiburg, Germany*
(Received 20 June 2017; published 14 August 2017)

We present a Monte Carlo simulation study of suspensions of hard ellipsoids of revolution. Based on the spatial fluctuations of the orientational order, we have computed the Frank elastic constants for prolate and oblate ellipsoids and compared them to the affine transformation model. The affine transformation model predicts the right order of magnitude of the twist and bend constant but not of the splay constant. In addition, we report the observation of a stable nematic phase at an aspect ratio as low as 2.5.

DOI: 10.1103/PhysRevE.96.022708

I. INTRODUCTION

The structure of a liquid—be its constituents atomic, molecular, or colloidal—is determined by an interplay of the attractive forces between the particles and the repulsion due to their excluded volumes. In the context of research on colloidal suspensions it is common to study the effect of the excluded volume separately from the attractive interactions by focusing on hard particle models [1]. This approach has been particularly successful in the case of anisotropic molecules and colloids, which form liquid crystalline phases [2]. One model system that has received considerable attention in the literature [3–28] is the suspension of hard ellipsoids of revolution (spheroids). Despite this large number of studies, there are still interesting aspects of the phase diagram as well as the materials properties of this system that have not been addressed. The aim of our paper is to fill some gaps in the literature. In particular, we discuss the phase behavior for a short aspect ratio that has not received attention yet—surprisingly, as it lies in a range that contains the limits of stability of at least two phases. And we present computer simulation results on the elastic properties of the nematic phase, which can serve as benchmarks for theoretical treatments of the system, e.g., by density functional theory.

II. MODEL, DEFINITIONS, AND ORDER PARAMETERS

We carried out Monte Carlo (MC) simulations of hard ellipsoids, i.e., the interaction potential was $V_{ij} = 0$ if the ellipsoids i and j did not overlap and $V_{ij} = \infty$ if they did. Overlaps were detected using the algorithm developed by Vieillard-Baron [29]. The phase diagram of this system is determined by the aspect ratio e and the volume fraction φ, where the aspect ratio is defined as $e = a/b$; a is the length of the high-symmetry axis and b is the length of the low-symmetry axis, and the volume fraction is $\varphi = N V_{\text{ell}}/V_{\text{box}}$ with V_{ell} the volume occupied by one ellipsoid and V_{box} the volume of the simulation box. As the system is formed by hard particles, temperature does not have an effect on the phase diagram, because the interaction potential is either zero or infinite.

In order to detect global orientational ordering, we computed S, the thermal average of the largest eigenvalue of the orientational order tensor defined as $Q_{ij} \equiv \frac{3}{2N}\sum_{\alpha=1}^{N}(u_\alpha^i u_\alpha^j - \frac{1}{3}\delta_{ij})$ where $\vec{u}_\alpha$ is the orientation of the particle α. To quantify global positional ordering in the system, we compute the bond-orientational order parameter Q_6 [30]: For each particle, we identify all the particles that are closer than a certain cut-off radius R_c from the first particle. All these particles are considered to be neighbors of the first particle. The cut-off radius is set to the distance at which the radial distribution function $g(r)$ passes through its first minimum. A bond is then defined between each couple of neighboring particles and to each bonds $\vec{r}$ the value $Q_{6m}(\vec{r}) = Y_{6m}[\theta(\vec{r}),\phi(\vec{r})]$ is associated where $\vec{r}$ is the center-to-center vector of the two neighboring particles and Y_{6m} are the spherical harmonics. The global bond-orientational order parameter Q_6 is then given by

$$Q_6 = \left(\frac{4\pi}{13}\sum_{m=-6}^{6}|\bar{Q}_{6m}|^2\right)^{1/2}\sqrt{N_b}, \tag{1}$$

where $\bar{Q}_{6m}$ is equal to the average of $Q_{6m}(\vec{r})$ over all the bonds between neighboring particles and N_b is the total number of bonds. (Here we follow the authors of Ref. [31] that showed that Q_6 converges to $1/\sqrt{N_b}$ in the isotropic phase and suggested to multiply Q_6 by $\sqrt{N_b}$ in order to make sure that Q_6 converges to 1 in the isotropic liquid phase and is much larger than 1 in crystalline systems.) We define the unitless reduced pressure P^* as $P^* = P\frac{8ab^2}{k_BT}$.

III. FRANK ELASTIC CONSTANTS

In the framework of the theory of elastic director fluctuations introduced by Frank [32], the free-energy cost of slowly varying spatial director-field inhomogeneity is given by

$$\mathcal{F} = \frac{1}{2}\int d^3\vec{r}\{K_1[\vec{\nabla}\cdot\vec{n}(\vec{r})]^2 + K_2[\vec{n}(\vec{r})\cdot(\vec{\nabla}\times\vec{n}(\vec{r}))]^2 + K_3[\vec{n}(\vec{r})\times(\vec{\nabla}\times\vec{n}(\vec{r}))]^2\}, \tag{2}$$

where K_1, K_2, and K_3 are the splay, twist, and bend Frank elastic constants, respectively.

As the elastic properties of liquid crystals are important for the switching process of liquid crystal displays, theoretical predictions of these constants for specific substances are of technological interest. To test theoretical approaches such as, e.g., density functional theory, hard ellipsoids are a useful model system. We have therefore extracted the values of K_1, K_2, and K_3 from our simulations in order to provide

benchmark data for comparison with theories. We used a method introduced by Allen and co-workers [17–20,33–35]. We briefly recapitulate the method in the following and refer the reader to Ref. [34] for a detailed description.

A. Order tensor fluctuations

The nematic order tensor of a spatially inhomogeneous director field is defined as

$$Q_{ij}(\vec{r}) := \frac{3}{2N}\sum_{\alpha=1}^{N}\left(u_\alpha^i u_\alpha^j - \frac{1}{3}\delta_{ij}\right)\delta(\vec{r}-\vec{r}_\alpha), \tag{3}$$

where $\vec{u}_\alpha$ is the orientation of the particle α and $i,j = 1,2,3$ are the three axes of the reference system. We orient the frame of reference $\{\vec{1},\vec{2},\vec{3}\}$ such that $\vec{3}$ direction is along the mean director field of the nematic phase, and we consider the Fourier transformed of Eq. (3) in this frame.

For long wavelength fluctuations of the order tensor and thus for low k values, the Fourier components of the order tensor are related to those of the director field [36],

$$\langle|\tilde{Q}_{\mu 3}(\vec{k})|\rangle^2 = \tfrac{9}{4}S^2\langle|\tilde{n}_\mu(\vec{k})|\rangle^2, \tag{4}$$

where $\mu = 1,2$ and $\tilde{\vec{n}}(\vec{k})$ is the Fourier transformed of $\vec{n}(\vec{r})$. For small variations of $\vec{n}$, the Frank free energy given in Eq. (2) can be written as

$$\begin{aligned}\mathcal{F} &= \frac{1}{2V}\sum_{\vec{k}}\left\{K_1k_1^2|\tilde{n}_1(\vec{k})|^2 + K_2k_1^2|\tilde{n}_2(\vec{k})|^2\right.\\ &\quad\left.+\left(K_3k_3^2+2\phi\right)[|\tilde{n}_1(\vec{k})|^2+|\tilde{n}_2(\vec{k})|^2]\right\}\\ &= \frac{1}{2V}\sum_{\vec{k}}\sum_{\mu=1}^{2}\left[K_\mu k_1^2 + K_3k_3^2 + 2\phi\right]|\tilde{n}_\mu(\vec{k})|^2,\end{aligned} \tag{5}$$

where ϕ is the strength of a small orienting field in order to restrain the average direction along the $\vec{3}$ direction. Each deformation mode contributes with an average energy of $k_BT/2$ to the free energy and thus,

$$\langle|\tilde{n}_\mu(\vec{k})|^2\rangle = \frac{Vk_BT}{K_\mu k_1^2 + K_3k_3^2 + 2\phi}, \quad \mu = 1,2. \tag{6}$$

Combining Eqs. (4) and (6) yields

$$\langle|\widetilde{Q}_{\mu 3}(\vec{k})|^2\rangle = \frac{\frac{9}{4}S^2Vk_BT}{K_\mu k_1^2 + K_3k_3^2 + 2\phi}, \quad \mu = 1,2. \tag{7}$$

We then define functions $W_{\mu 3}(\vec{k})$:

$$W_{\mu 3}(\vec{k}) \equiv \frac{\frac{9}{4}S^2Vk_BT}{\langle|\widetilde{Q}_{\mu 3}(\vec{k})|^2\rangle} \to K_\mu k_1^2 + K_3k_3^2 + 2\phi, \quad \text{as} \quad k\to 0. \tag{8}$$

Equation (8) builds a bridge between the Frank elastic constants K_1, K_2, and K_3 and the quantity $W_{\mu 3}(\vec{k})$ which can be sampled in simulations. In order to extract the elastic constants from (8), $W_{\mu 3}(\vec{k})$ is fitted to polynomials in k_1^2 or k_3^2 while the other coordinate is fixed.

In the limit of high k values, the function $W_{\mu 3}(\vec{k})$ converges to a limiting value [34,35],

$$W_{\mu 3}(\vec{k}) \to \frac{\langle P_2^2\rangle\rho k_BT}{\frac{1}{21}\langle P_2\rangle - \frac{4}{35}\langle P_4\rangle + \frac{1}{15}}, \quad \text{as} \quad k\to\infty, \tag{9}$$

where P_2 is the second-order and P_4 the fourth-order Legendre polynomial of $\vec{u}_i\cdot\vec{n}$.

In order to use Eq. (8) introduced in the previous section, we have to ensure that the mean director field stays close to the $\vec{3}$ direction during the simulation. As recommended in [34,35], we use a weak external field for that purpose. Especially for oblate particles, the use of the external field turned out to be indispensable.

In order to facilitate the implementation of the computation of $\langle|\widetilde{Q}_{\mu 3}(\vec{k})|^2\rangle$, one can compute analytically the squared modulus of $Q_{\mu 3}$. A straightforward calculation leads to

$$\begin{aligned}|\widetilde{Q}_{\mu 3}(\vec{k})|^2 = \left(\frac{3V}{2N}\right)^2\left\{\left[\sum_{i=1}^{N}u_{i\mu}u_{i3}\cos(\vec{k}\cdot\vec{r}_i)\right]^2\right.\\ \left.+\left[\sum_{i=1}^{N}u_{i\mu}u_{i3}\sin(\vec{k}\cdot\vec{r}_i)\right]^2\right\}.\end{aligned} \tag{10}$$

The k space is discretized such that the wave vectors are given by

$$\vec{k} = k_0(\kappa_1,0,\kappa_3) \tag{11}$$

with $k_0 = 2\pi/L$ where L is the length of the simulation box and κ_1 and κ_3 are positive integers. The maximal values of κ_1 and κ_3 have to be chosen such that in the high k-value limit $W_{\mu 3}(\vec{k})$ converges according to (9). In our simulations this was achieved for $\kappa_{\max}\sim 100$.

In order to estimate the statistical error of $W_{\mu 3}(\vec{k})$, we saved $W_{\mu 3}(\vec{k})$ after a given number of Monte Carlo steps and used the mean value computed over these blocks to determine the Frank elastic constants. The final step in the determination of the Frank elastic constants is to fit $W_{\mu 3}(\vec{k})$ to polynomials in k_1 and k_3. The leading coefficients for $k\to 0$ determine the Frank elastic constants according to Eq. (8).

B. Affine transformation model

Osipov and Hess [37] derived expressions for the Frank elastic constants using the approximation of perfect local orientational order and the assumption that the properties of the hard-ellipsoid system can be obtained from the properties of the hard-sphere system using an affine transformation:

$$K_1 = \bar{K}\{1+\Delta-9\Delta(S_4/S)+[39/11\Delta+6](S_4/S)^2\}. \tag{12}$$

$$K_2 = \bar{K}\{1-2\Delta-3\Delta(S_4/S)+[-141/11\Delta+6](S_4/S)^2\}, \tag{13}$$

$$K_3 = \bar{K}\{1+\Delta+12\Delta(S_4/S)+[102/11\Delta+6](S_4/S)^2\}, \tag{14}$$

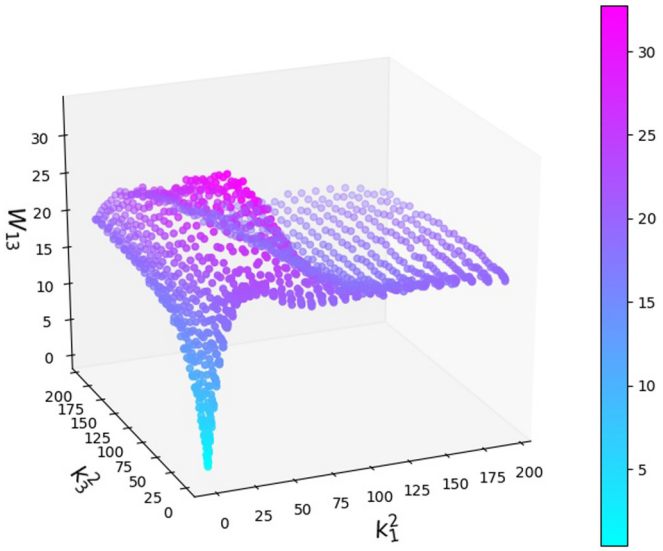

FIG. 1. The function $W_{13}(\vec{k})$ for a system of hard ellipsoids of aspect ratio 0.2 at the volume fraction $\varphi = 0.360$.

where

$$\Delta = \frac{2\,e^2 - 1}{7\,e^2 + 1} \tag{15}$$

and $\bar{K}$ depends on $\bar{S}_4/\bar{S}$, the aspect ratio e, and the direct correlation function of the hard-sphere fluid at the same volume fraction as the hard-ellipsoid fluid. $\bar{S}_4$ is defined as $\bar{S}_4 = \langle P_4(\cos\theta)\rangle$ where θ is the angle between a particle and the local director and $\langle\cdots\rangle$ corresponds to the average over all the particles.

Adding the three equations in (14) allows one to express $\bar{K}$ in terms of K_1, K_2, K_3, and S_4/S,

$$\bar{K} = \frac{K_1 + K_2 + K_3}{3 + 18\left(\frac{S_4}{S}\right)^2}. \tag{16}$$

Equation (16) can be used together with the data from the simulations or from experiments in order to determine $\bar{K}$. In the following we will compare our simulation results to these approximate theoretical expressions.

C. Results

We used two systems of prolate ellipsoids of aspect ratio 5.0 and 2.5 and a system of oblate ellipsoids of aspect ratio 0.2. The systems contained roughly 11 000 particles and the simulations were ran in the NVT ensemble. Each run is equilibrated over $\sim 3 \times 10^6$ Monte Carlo steps where 1 MC step consists of one trial move per particle on average. After the equilibration, the functions $W_{13}(\vec{k})$ and $W_{23}(\vec{k})$ are sampled over $\sim 2 \times 10^6$ Monte Carlo steps. Figure 1 shows $W_{13}(\vec{k})$ for the aspect ratio 0.2 at the volume fraction $\varphi = 0.360$. The function $W_{13}(\vec{k})$ converges for large k values and goes to zero for small k values. Polynomial fits of $W_{13}(\vec{k})$ or $W_{23}(\vec{k})$ in terms of k_1^2 and k_2^2 are used to determine the Frank elastic constants according to Eq. (8).

The Frank elastic constants for the aspect ratio 0.2, 2.5, and 5.0 are given in the Appendix. At those volume fractions, for which Tjipto-Margo *et al.* [19] did simulations in 1992, our results for the Frank elastic constants are in agreement with their results (see Figs. 4 and 5).

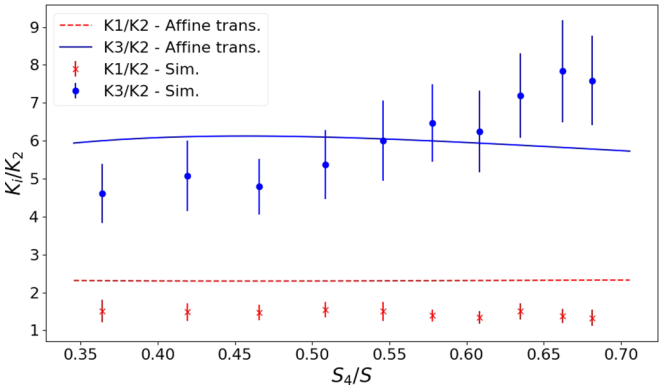

FIG. 2. Ratios of the Frank elastic constants as a function of S_4/S for aspect ratio 5.0. Solid line (blue) corresponds to the theoretical expression of K_3/K_2 given in Eq. (14) and data points (•) are from the simulations. Dashed line (red) corresponds to the theoretical expression of K_1/K_2 given in Eq. (14) and data points (×) are from the simulations.

Figures 2 and 3 compare ratios of the Frank elastic constants obtained from our simulations with the expressions of Eq. (14) for $e = 5.0$ and $e = 0.2$, respectively. For $e = 5.0$, the ratio K_1/K_2 (dashed line and crosses) is always overestimated by the theory and the ratio K_3/K_2 (solid line and filled circles) is overestimated at low values of S_4/S and underestimated at high values of S_4/S. However, note that the easy-to-use expressions in Eq. (14) allow one to estimate the correct orders of magnitude of the ratios of the Frank elastic constants. For $e = 0.2$, the theoretical curve of the ratio K_1/K_2 (dashed line and crosses) is in very good agreement with data obtained from the simulations and the ratio K_3/K_2 (solid line and filled circles) is overestimated by the theory. In order to directly compare the values for the Frank elastic constants obtained

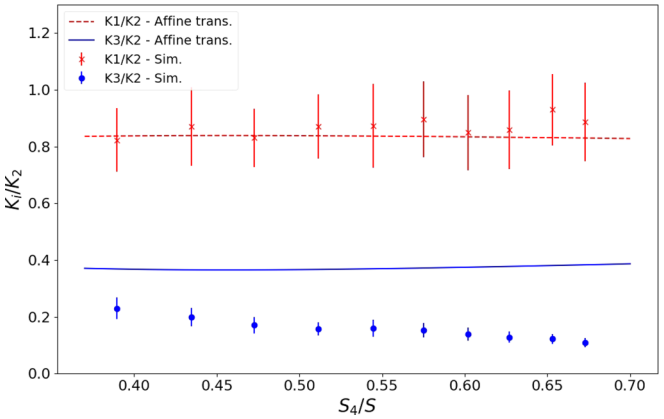

FIG. 3. Ratios of the Frank elastic constants as a function of S_4/S for aspect ratio 0.2. Solid line (blue) corresponds to the theoretical expression of K_3/K_2 given in Eq. (14) and data points (•) are from the simulations. Dashed line (red) corresponds to the theoretical expression of K_1/K_2 given in Eq. (14) and data points (×) are from the simulations.

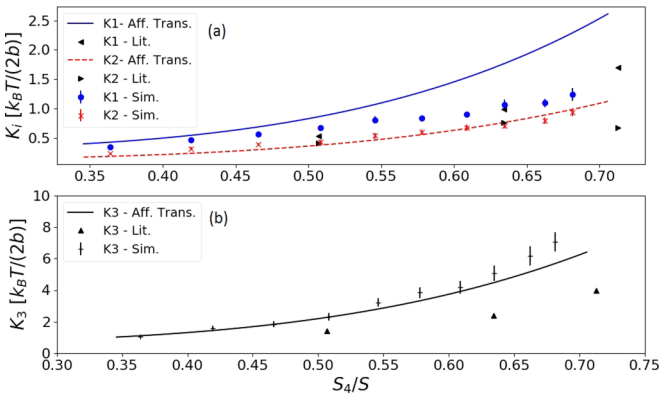

FIG. 4. Frank elastic constants as a function of S_4/S for $e = 5.0$: K_1 and K_2 in (a) and K_3 in (b). Lines correspond to the expressions given in Eq. (14) and data points are from the simulations; triangles indicate the data from Tjipto-Margo *et al.* [19].

from the simulations and the theory, we have determined $\bar{K}$ using Eq. (16). We used the data from the simulations in order to compute $\bar{K}$ for certain values of S_4/S. These data points were then fitted to determine $\bar{K}$ for any value of S_4/S.

The knowledge of $\bar{K}$ allows us to plot the Frank elastic constants as a function of S_4/S. These plots are shown in Fig. 4 for $e = 5.0$ and in Fig. 5 for $e = 0.2$. In addition to our results, we also show the values of the Frank elastic constants measured by Tjipto-Margo *et al.* [19]. For $e = 5.0$, the twist (K_2) and bend (K_3) constants are in good agreement with the simulations and the splay (K_1) constant is overestimated by the theory. In the derivation of the expressions of Eq. (14) the authors of [37] applied the perfect local alignment approximation. As the splay deformation is a local deformation, the free-energy cost associated to such a splay deformation is highly overestimated by the theory based on the perfect local alignment approximation.

For $e = 0.2$, the splay (K_1) and twist (K_2) constants are slightly underestimated by the theory as it is shown in Fig. 5. As both constants are underestimated, the ratio of K_1/K_2 is in very good agreement with the data from the simulations as shown

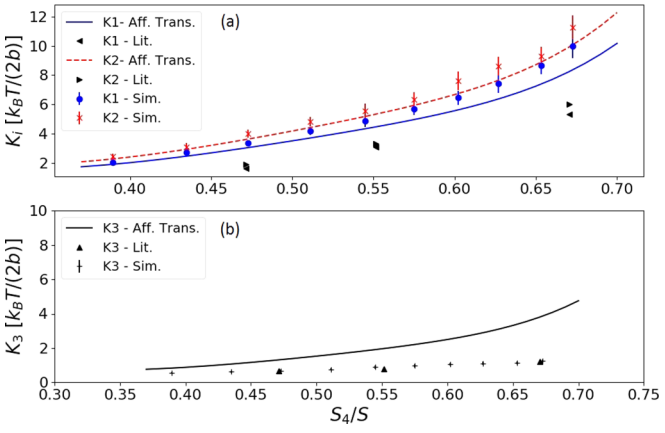

FIG. 5. Frank elastic constants as a function of S_4/S for $e = 0.2$: K_1 and K_2 in (a) and K_3 in (b). Lines correspond to the expressions given in Eq. (14) and data points are from the simulations; triangles indicate the data from Tjipto-Margo *et al.* [19].

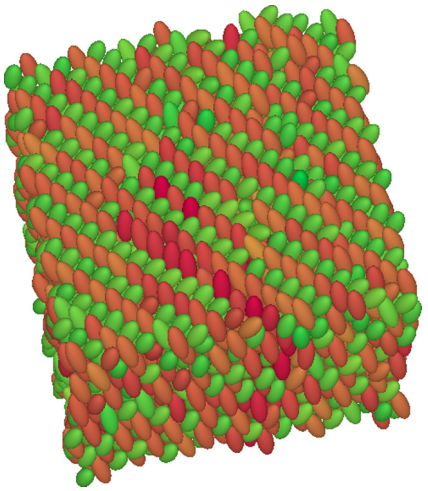

FIG. 6. Snapshots of the SM2 crystal for aspect ratio 2.5. The colors indicate the two preferred orientations.

in Fig. 3. The bend constant (K_3) is strongly overestimated by the affine transformation model and for the constant the theory is not even able to describe correctly the order of magnitude.

IV. UPDATE OF THE PHASE BOUNDARY

Since the first version of the phase diagram of the hard ellipsoid model was proposed by Frenkel *et al.* [3,4] many updates have been published [5–7]. Still there remain questions about the phase behavior, as e.g., at which aspect ratio the isotropic-nematic phase transition ends (there is obviously no nematic phase in a system of spheres, while there is one for strongly anisotropic ellipsoids, thus the transition region needs to disappear at some aspect ratio $e > 1$); if isotropic-nematic coexistence could end in a critical point or if at a particular aspect ratio the transition from the liquid to a crystal phase takes over, and if so, which crystal phase that might be.

As the isotropic-nematic phase transition has been observed in simulations for $e = 2.75$, but not for $e = 2.00$ [3,4], we know that this phase coexistence region ends in the range of $e \in]2.00, 2.75[$. For hard ellipsoids with low asymmetry, a phase transition between the stretched face-centered-cubic (sfcc) crystal and the simple monoclinic with two orientations

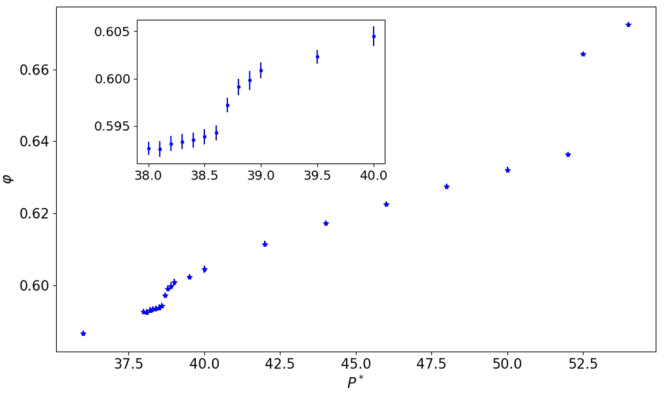

FIG. 7. Volume fraction φ as a function of the reduced pressure P^* for $e = 2.5$.Two jumps indicate two phase transitions. The inset shows a zoom-in on the region of $P^* \in [38.00, 40.00]$.

(SM2) crystal was found [5,7]. (A snapshot of the SM2 phase is shown in Fig. 6.) While in the sfcc crystal all the particles align in one direction, on average, in the SM2 crystal two preferred directions exist. As far as we know the phase boundaries of this transition are not yet determined and there might be a sfcc-SM2 transition for $e \in]2.00,2.75[$.

In order to investigate this region of the phase diagram for which only little information is available [8], we have performed Monte Carlo simulations for $e = 2.50$ in a system of $N = 3281$ particles and in the NPT ensemble. All the simulations were started from the sfcc crystal and equilibrated at the different pressures for 2×10^8 MC steps, where one MC step consists on average of N translation or orientation moves and one volume move. After equilibration, the data was sampled over approximately 10^7 MC steps. In order to identify the different phases present at $e = 2.50$ we have sampled the volume fraction φ, the nematic order parameter S, the bond-orientational order parameter Q_6, the radial distribution function $g(r)$, and the orientational pair-correlation function $g_2(r)$.

The volume fraction φ as a function of the reduced pressure P^* is shown in Fig. 7. There are two discontinuities, indicating two phase transitions. The first transition takes place at approximately $P^* = 38.60$ (a preliminary analysis of larger systems indicated that the transition shifts to $38.8 < P^*_{\mathrm{IN}} < 39.0$) and the second transition at $P^* = 52.50$. Figure 8 shows Q_6 as a function of the reduced pressure. It shows that for reduced pressures $P^* < 52.50$ the system is liquid and for larger reduced pressures the system is crystalline. In order to identify the first phase transition and determine if the crystal formed at high pressures is an sfcc crystal or an SM2 crystal we show the nematic order parameter S as a function of the pressure (see Fig. 9). S strongly increases near $P^* = 38.60$ and slightly decreases at $P^* = 52.50$. The first phase transition is thus the isotropic-nematic phase transition, and the small decrease of the nematic order parameter S indicates the formation of the SM2 crystal, which has less pronounced alignment than the sfcc phase. (In the stretched centered-cubic crystal all the particles are pointing in the same direction on average, while in the SM2 crystal two preferred directions exist which leads to a decrease of the nematic order parameter S.) Thus, the information given in Figs. 7, 8, and 9

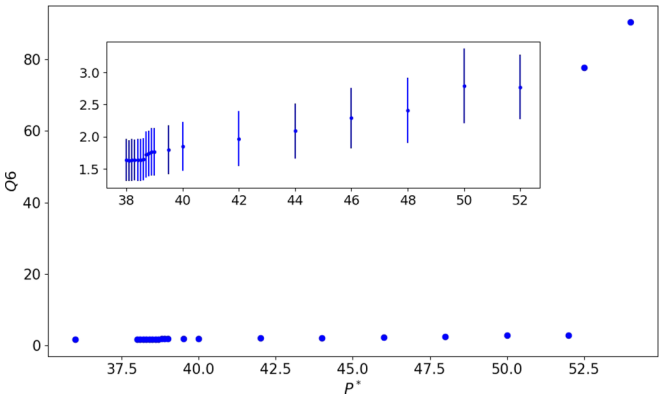

FIG. 8. Bond-orientational order parameter Q_6 as a function of the reduced pressure P^* for $e = 2.5$. Large change of Q_6 near $P^* = 52.50$. Inset shows a zoom-in on the region of $P^* \in [38.00,52.00]$.

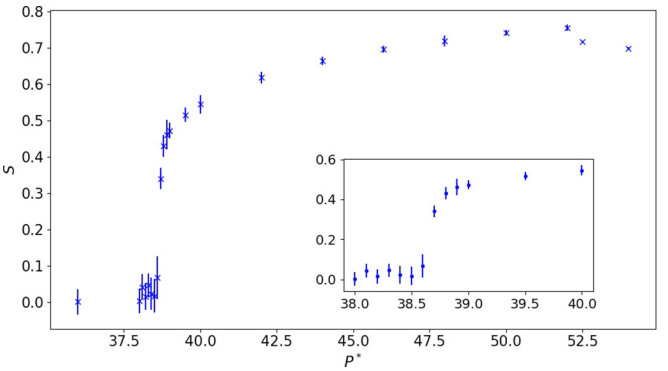

FIG. 9. Nematic order parameter S as a function of the pressure for $e = 2.5$. Strong variation of the S near $P^* = 38.60$ and noticeable decrease of S near $P^* = 52.50$. Inset shows a zoom-in on the region of $P^* \in [38.00,40.00]$.

gives evidence that for $P^* < 38.60$ the system is isotropic, for $P^* \in]38.60,52.50[$ the system is nematic, and for $P^* > 52.50$ the SM2 crystal is stable. We conclude that for $e = 2.50$ the nematic phase is still observable and the liquid-crystal transition leads to the SM2 crystal and not to the sfcc crystal.

V. SUMMARY

We have presented a Monte Carlo simulations study of hard ellipsoids. We find that for aspect ratio $e = 2.5$ there is still a range of pressures in which the nematic phase is stable. At high pressures, the nematic phase crystallizes into the SM2 phase. Further we have computed the Frank elastic constants for prolate and oblate ellipsoids and compared them to the affine transformation model. The affine transformation model predicts the right order of magnitude for the bend and twist constant but not for the splay constant.

APPENDIX: FRANK ELASTIC CONSTANTS: DATA

Here we present the Frank elastic constants obtained from the order tensor fluctuations plotted in Sec. III C. The tables contain the volume fraction φ, the nematic order parameter S, the fourth-order Legendre polynomial P_4, and the three Frank elastic constants with associated errors.

TABLE I. Aspect ratio 0.2: Splay (K_1), twist (K_2), and bend (K_3) elastic constants; volume fraction (φ); nematic order parameter (S); fourth-order Legendre polynomial (P_4).

φ	S	P_4	K_1	ΔK_1	K_2	ΔK_2	K_3	ΔK_3
0.36	0.620	0.242	2.0	0.1	2.4	0.2	0.56	0.05
0.37	0.667	0.290	2.7	0.2	3.1	0.2	0.62	0.05
0.38	0.703	0.332	3.3	0.2	4.0	0.3	0.69	0.07
0.39	0.732	0.374	4.1	0.3	4.8	0.3	0.76	0.06
0.40	0.757	0.412	4.8	0.4	5.6	0.5	0.89	0.08
0.41	0.779	0.448	5.7	0.4	6.3	0.5	0.97	0.08
0.42	0.796	0.479	6.5	0.5	7.6	0.6	1.07	0.09
0.43	0.813	0.510	7.4	0.6	8.6	0.6	1.11	0.09
0.44	0.828	0.541	8.7	0.6	9.3	0.6	1.15	0.08
0.45	0.840	0.565	10.0	0.8	11.3	0.8	1.24	0.09

TABLE II. Aspect ratio 5.0: Splay (K_1), twist (K_2), and bend (K_3) elastic constants; volume fraction (φ); nematic order parameter (S); fourth-order Legendre polynomial (P_4).

φ	S	P_4	K_1	ΔK_1	K_2	ΔK_2	K_3	ΔK_3
0.38	0.568	0.207	0.35	0.04	0.23	0.02	1.1	0.1
0.39	0.642	0.269	0.47	0.03	0.31	0.03	1.6	0.2
0.40	0.692	0.322	0.56	0.05	0.38	0.02	1.8	0.2
0.41	0.728	0.370	0.67	0.04	0.43	0.03	2.3	0.2
0.42	0.756	0.413	0.81	0.06	0.54	0.05	3.2	0.3
0.43	0.778	0.450	0.83	0.04	0.60	0.04	3.9	0.4
0.44	0.800	0.487	0.91	0.05	0.67	0.05	4.2	0.4
0.45	0.816	0.518	1.06	0.09	0.71	0.04	5.1	0.5
0.46	0.832	0.551	1.10	0.07	0.79	0.06	6.2	0.6
0.47	0.844	0.575	1.24	0.11	0.93	0.07	7.1	0.6

TABLE III. Aspect ratio 2.5: Splay (K_1), twist (K_2), and bend (K_3) elastic constants; volume fraction (φ); nematic order parameter (S); fourth-order Legendre polynomial (P_4).

φ	S	P_4	K_1	ΔK_1	K_2	ΔK_2	K_3	ΔK_3
0.600	0.555	0.190	0.53	0.06	0.43	0.04	1.36	0.12
0.605	0.617	0.237	0.65	0.05	0.51	0.05	1.92	0.17
0.610	0.660	0.281	0.81	0.07	0.65	0.06	2.18	0.27
0.615	0.681	0.307	1.06	0.11	0.84	0.08	2.83	0.26
0.620	0.710	0.347	1.12	0.16	0.97	0.10	3.25	0.38

[1] R. A. L. Jones, *Soft Condensed Matter* (Oxford University Press, Oxford, 2002).
[2] L. Onsager, Ann. NY Acad. Sci. **51**, 627 (1949).
[3] D. Frenkel, B. M. Mulder, and J. P. McTague, Phys. Rev. Lett. **52**, 287 (1984).
[4] D. Frenkel and B. M. Mulder, Mol. Phys. **55**, 1171 (1985).
[5] P. Pfleiderer and T. Schilling, Phys. Rev. E **75**, 020402 (2007).
[6] G. Odriozola, J. Chem. Phys. **136**, 134505 (2012).
[7] G. Bautista-Carbajal, A. Moncho-Jord, and G. Odriozola, J. Chem. Phys. **138**, 064501 (2013).
[8] M. Han, L. Yao, L. Sheng, X. Hai-Guang, and M. Hong-Ru, Chin. Phys. Lett. **32**, 026401 (2015).
[9] A. Donev, F. H. Stillinger, P. M. Chaikin, and S. Torquato, Phys. Rev. Lett. **92**, 255506 (2004).
[10] E. De Miguel and M. P. Allen, Mol. Phys. **76**, 1275 (1992).
[11] G. Cinacchi and F. Schmid, J. Phys.: Condens. Matter **14**, 12223 (2002).
[12] A. J. McDonald, M. P. Allen, and F. Schmid, Phys. Rev. E **63**, 010701 (2000).
[13] D. Andrienko, G. Germano, and M. P. Allen, Phys. Rev. E **62**, 6688 (2000).
[14] S. Dorosz, N. Shegokar, T. Schilling, and M. Oettel, Soft Matter **10**, 4717 (2014).
[15] M. Letz and A. Latz, Phys. Rev. E **60**, 5865 (1999).
[16] A. Avazpour, V. Mahdavi, and L. Avazpour, Phys. Rev. E **82**, 041701 (2010).
[17] M. P. Allen and D. Frenkel, Phys. Rev. A **37**, 1813(R) (1988).
[18] M. P. Allen and D. Frenkel, Phys. Rev. A **42**, 3641 (1990).
[19] B. Tjipto-Margo, G. T. Evans, M. P. Allen, and D. Frenkel, J. Phys. Chem. **96**, 3942 (1992).
[20] N. H. Phuong, G. Germano, and F. Schmid, J. Phys. Chem. **115**, 7227 (2001).
[21] J. M. Bricker, H. O. Park, and J. E. Butler, J. Rheol. (NY) **52**, 941 (2008).
[22] A. P. Cohen, S. Dorosz, A. B. Schofield, T. Schilling, and E. Sloutskin, Phys. Rev. Lett. **116**, 098001 (2016).
[23] D. Florea and H. M. Wyss, J. Colloid Interface Sci. **416**, 30 (2014).
[24] D. Schneider, P. J. Beltramo, M. Mattarelli, P. Pfleiderer, J. Vermant, D. Crespy, M. Montagna, E. M. Furst, and G. Fytas, Soft Matter. **9**, 9129 (2013).
[25] A. P. Cohen, E. Janai, E. Mogilko, A. B. Schofield, and E. Sloutskin, Phys. Rev. Lett. **107**, 238301 (2011).
[26] B. Madivala, J. Fransaer, and J. Vermant, Langmuir **25**, 2718 (2009).
[27] P. Pfleiderer, K. Milinkovic, and T. Schilling, Europhys. Lett. **84**, 16003 (2008).
[28] S. Dorosz and T. Schilling, J. Chem. Phys. **139**, 124508 (2013).
[29] J. Vieillard-Baron, J. Chem. Phys. **56**, 4729 (1972).
[30] P. J. Steinhardt, D. R. Nelson, and M. Ronchetti, Phys. Rev. B **28**, 784 (1983).
[31] M. D. Rintoul and S. Torquato, J. Chem. Phys. **105**, 9258 (1996).
[32] F. C. Frank, Discuss. Faraday Soc. **25**, 19 (1958).
[33] M. P. Allen, M. A. Warren, M. R. Wilson, A. Sauron, and W. Smith, J. Chem. Phys. **105**, 2850 (1996).
[34] P. A. O'Brien, M. P. Allen, D. L. Cheung, M. Dennison, and A. Masters, Phys. Rev. E **78**, 051705 (2008).
[35] P. A. O'Brien, M. P. Allen, D. L. Cheung, M. Dennison, and A. Masters, Soft Matter **7**, 153 (2011).
[36] D. Forster, Ann. Phys. (NY) **84**, 505 (1974).
[37] M. A. Osipov and S. Hess, Mol. Phys. **78**, 1191 (1993).